ARL-TR-10099 ● MAY 2025

Polyurethane Chemorheological Analysis for In Situ Ambient Reactive Extrusion Additive Manufacturing

by Alice Savage, Aynslie J. Fritz, Nicholas Enos, Jeffrey Wiggins, Ian McAninch, and E. Jason Robinette

NOTICES

Disclaimers

The findings in this report are not to be construed as an official Department of the Army position unless so designated by other authorized documents.

Citation of manufacturer's or trade names does not constitute an official endorsement or approval of the use thereof.

Destroy this report when it is no longer needed. Do not return it to the originator.

ARL-TR-10099 ● MAY 2025

Polyurethane Chemorheological Analysis for In Situ Ambient Reactive Extrusion Additive Manufacturing

Alice Savage, Ian McAninch, and E. Jason Robinette
DEVCOM Army Research Laboratory

Aynslie J. Fritz, Nicholas Enos, and Jeffrey Wiggins
University of Southern Mississippi

REPORT DOCUMENTATION PAGE

1. REPORT DATE	2. REPORT TYPE	3. DATES COVERED	
		START DATE	END DATE
May 2025	Technical Report	9/30/2019	9/29/2021

4. TITLE AND SUBTITLE
Polyurethane Chemorheological Analysis for In Situ Ambient Reactive Extrusion Additive Manufacturing

5a. CONTRACT NUMBER	5b. GRANT NUMBER	5c. PROGRAM ELEMENT NUMBER
5d. PROJECT NUMBER W911NF-18-2-0061	**5e. TASK NUMBER**	**5f. WORK UNIT NUMBER**

6. AUTHOR(S)
Alice Savage, Aynslie J. Fritz, Nicholas Enos, Jeffrey Wiggins, Ian McAninch, and E. Jason Robinette

7. PERFORMING ORGANIZATION NAME(S) AND ADDRESS(ES)	8. PERFORMING ORGANIZATION REPORT NUMBER
DEVCOM Army Research Laboratory ATTN: FCDD-RLA-MG Aberdeen Proving Ground, MD 21005	ARL-TR-10099

9. SPONSORING/MONITORING AGENCY NAME(S) AND ADDRESS(ES)	10. SPONSOR/MONITOR'S ACRONYM(S)	11. SPONSOR/MONITOR'S REPORT NUMBER(S)

12. DISTRIBUTION/AVAILABILITY STATEMENT
DISTRIBUTION STATEMENT A. Approved for public release: distribution unlimited.

13. SUPPLEMENTARY NOTES
ORCIDs: Alice Savage, 0000-0003-0167-4966; Ian McAninch, 0000-0002-9190-2936; Jason Robinette, 0000-0003-4096-8502

14. ABSTRACT
A parallel study of polyurethane (PU) chemorheological properties and their subsequent 3D printing via ambient reactive extrusion (ARE) additive manufacturing (AM) is reported. PU modularity makes them promising feedstock for ARE, thus the chemorheological properties of PUs with systematically increased concentrations of fumed silica (FS) were evaluated. Unfilled PUs displayed the longest gel time (51 min), while increasing FS concentration decreased gel time to 16–28 min. The first PUs printed via ARE in available open literature were demonstrated with 5.0 wt% FS PUs, where printed specimens agreed with intended geometry and achieved vertical heights exceeding 25 mm. Cross-sectional analysis via optical microscopy and scanning electron microscopy revealed coalescence of deposited layers with no distinct interfaces. Specimen were post-cured at 160 °C for 2 h, where hard segment glass transition temperature was observed to increase from 67.9 to 74.1 °C. The unique simultaneous synthesis and 3D printing strategy utilized in this research combined chemorheological analysis and successful PU print demonstrations to establish an ARE platform for further reactive materials and 3D printing applications.

15. SUBJECT TERMS
Sciences of Extreme Materials, additive manufacturing, polyurethane, reactive extrusion, fused filament fabrication

16. SECURITY CLASSIFICATION OF:			17. LIMITATION OF ABSTRACT	18. NUMBER OF PAGES
a. REPORT	b. ABSTRACT	C. THIS PAGE		
UNCLASSIFIED	UNCLASSIFIED	UNCLASSIFIED	UU	38

19a. NAME OF RESPONSIBLE PERSON	19b. PHONE NUMBER *(Include area code)*
Alice Savage	(520) 691-4776

STANDARD FORM 298 (REV. 5/2020)
Prescribed by ANSI Std. Z39.18

Contents

List of Figures

List of Tables

Acknowledgments

We gratefully acknowledge the U.S. Army Research Laboratory Award No. W911NF-18-2-0061-P00002 for the financial support and collaboration of this research. We would also like to acknowledge Covestro Company for their kind donation of Desmodur VL R20, and Dwaine Braasch, Anthony Griffin, David Delatte, and Lina Ghanbari for experimental support.

1. Introduction

Additive manufacturing (AM) refers to the process of developing 3D objects through the deposition of material in an additive fashion.[1] Though originally utilized for rapid prototyping, AM has recently seen an increase in usage as an industrial manufacturing method due to its ability to produce complex geometries.[2] With the advent of extrusion-based AM methods such as Big Area Additive Manufacturing (BAAM), 3D printing of two-seat electric roadster cars[3] and wind turbine blade molds[4] have been realized. Each example enabled larger print volumes, faster print speeds, and decreased material expenses when compared to traditional extrusion AM processes. BAAM operates similarly to the common 3D printing method known as fused filament fabrication (FFF), whereby both methods use thermoplastic polymers (pellets for BAAM, filament for FFF) that are melted during extrusion and reconsolidated on the print bed.[5] Thermoplastic polymers are the only applicable polymers for these methods; thus, FFF and BAAM are reliant upon polymer chain entanglement across the deposited layers, making printed specimens susceptible to mechanical anisotropy.[5–7] Mechanical anisotropy refers to nonequivalent mechanical properties in the X, Y, and Z direction, with the Z direction often being the weakest point resulting from the layer-by-layer fashion of AM.

While first reported by Calvert et al.[8] in 1997, reactive AM (RAM) methods have recently gained increasing relevance due to their ability to fabricate 3D specimens via deposition, in situ polymerization, and subsequent post-cure of reactive inks. RAM has also been used to address mechanical anisotropy, through which in situ polymerization and post-cures of printed polymeric material promote interlayer polymerization. Using reactive direct ink writing, Compton and Lewis[9] observed full coalescence of deposited layers in epoxy-based cellular composites following the initial polymerization of reactive inks while printing and subsequent post-cures to complete polymerization. Rios et al.[10] introduced ambient reactive extrusion (ARE) as a large-scale RAM process capable of printing thermoset materials, wherein liquid monomers were individually stored and fed through a lightweight mixing nozzle prior to deposition. Through ARE, thermal stresses common in other AM methods were minimized due to ambient processing temperatures, while faster print speeds and larger volumes were feasible using lightweight hardware. The in situ cross-linking of the deposited reactive polymers yielded specimens that exhibited a higher elongation at break when compared to nonreactive thermoplastic specimens.[10] In 2021, Uitz et al.[11] established a version of ARE referred to as reactive extrusion additive manufacturing, in which a commercially available, reactive epoxy-amine system was simultaneously synthesized and printed.

Mechanical properties of the printed specimen in multiple orientations were evaluated and reported as having isotropic (equivalent) tensile modulus and ultimate strength, but anisotropic elongation at break and toughness. However, the exothermic nature of the polymerization while printing caused variations in degree of cure of the specimen, which led to variations in mechanical properties, causing the authors to report the results as a function of fracture mechanism (brittle vs ductile).[11]

Many efforts have focused on the advancement of AM processes for enhanced mechanical properties or producing large-scale parts. However, a simultaneous thrust is necessary to not only expand the library of 3D-printable polymers, but also understand the properties that deem materials printable. Polyurethanes (PUs) are attractive polymers for AM due to their modular chemistry and multifaceted tailorable properties. PUs are synthesized from the step growth polymerization of diisocyanates, macroglycols (polyols), and diol chain extenders. More specifically, PUs are characterized by the urethane repeat unit formed from the reaction between isocyanate and hydroxyl functionalities.[12,13] An extensive library of commercialized PU monomers exists due to PU applications in several industries (from biocompatible heart valves[14] to rigid ski boots).[15] Therefore, many AM methods, such as stereolithography (SLA), FFF, and direct ink writing (DIW), have designed and adapted PUs as printable materials.

The use of PUs in multiple AM processes highlights their processing versatility; for example, 3D-printed PUs have targeted numerous applications, such as the use of photo-polymerizable PUs (SLA) as elastic scaffolds for tissue engineering[16] or PU inks for sustainable DIW printing strategies.[17] Thermoplastic PUs (TPUs), a common feedstock for FFF, are commercially available as flexible filament, though they are often difficult to successfully print and require specialized TPU–FFF print heads.[18] In addition to PU modularity, PUs have an extensive history in reactive metering strategies, such as the use of reactive extrusion (REX) to simultaneously polymerize and extrude TPUs[19–21] or through reaction injection molding (RIM) of PUs.[22] The two-feed strategy common in REX and RIM has been adapted for reactive inkjet printing, in which reactive monomer inks, consisting of a hydroxyl side and isocyanate side, were consecutively deposited as sub-nanoliter droplets to yield urethane linkages across the layers.[23,24] However, in the study by Kröber et al.,[23] the solid PU prints were on the micron scale and required 3 to 5 min of cure time. This excessive cure time, by AM standards, was required to prevent the flow of initial layers prior to subsequent layer deposition. Though reactive ink jetting was successful for small PU prints and beneficial for applications that require higher spatial resolution, it was not broadly industrially relevant.

Open literature regarding the in situ polymerization of PUs using ARE remains sparse, despite PU modularity and an extensive history with REX-based processing techniques. Moreover, the relationship between polymer design and resultant chemorheological properties adapted for ARE is underexplored. Herein, we demonstrate the influence and importance of different PU components, such as additive concentrations, for achieving critical chemorheological properties required for in situ PU polymerization during 3D printing. Chemorheological properties of PUs containing systematically increased additive concentrations were first evaluated prior to demonstration and analysis of a representative PU printed via ARE. The twofold approach to quantitatively evaluating PU chemorheological properties for correlation with ARE PU print quality is highlighted in Figure 1.

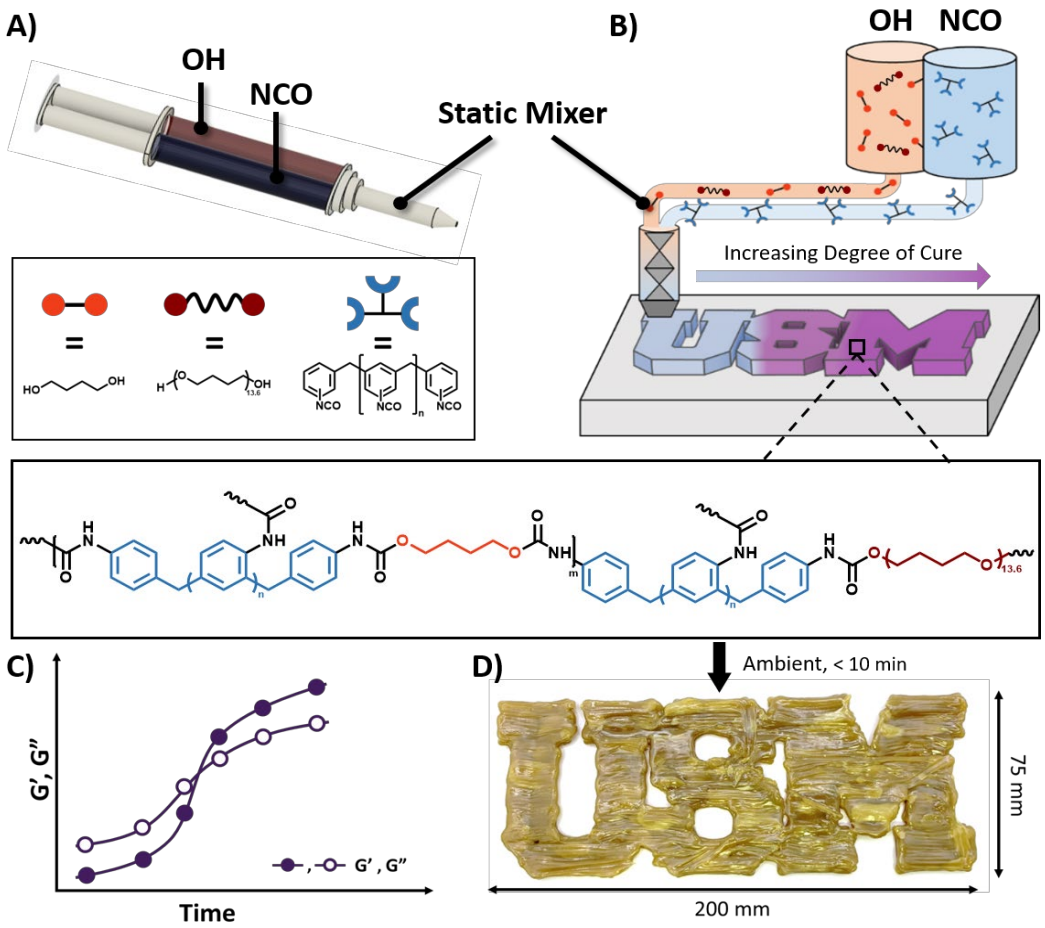

Figure 1. Experimental evaluation and 3D printing strategy for ARE of PUs. (A) Dual-component syringe with static mixer used for chemorheological characterization. (B) Two-component feed strategy of reactive components that begin polymerization upon mixing immediately prior to deposition. (C) Idealized chemorheological results compared to ARE print quality. (D) Image of ARE–3D printed PU consisting of three layers (192 mm long, 71 mm wide, and 4 mm high).

2. Materials and Methods

2.1 Materials

Polymeric 4,4'-diphenylmethane diisocyanate (pMDI) (Covestro, Desmodur VL R20, M_n ~ 400 g/mol), 1,4-butanediol (BD) (Sigma Aldrich), and dibutyltin dilaurate (DBTDL) (TCI Chemicals) were used as received. Polytetramethylene ether glycol (PTMEG) (Sigma Aldrich, M_n = 1000 g/mol) was dried under vacuum at 100 °C for a minimum of 3 h prior to use. Untreated, fumed colloidal silica (FS) (Strem Chemical, 99+%, specific surface area S_{ar} = 400 m^2/g) was heated under vacuum at 150 °C for 4 h to remove moisture, cooled to ambient temperature under vacuum, and stored in desiccators until used. Desmodur VL R20 was generously donated by Covestro.

2.2 Synthesis of Fumed Silica-Polyurethanes Using Dual-Component Syringe

Synthesized PUs for this study specifically corresponded to a 1:1 volumetric feed ratio of hydroxide (OH) to isocyanate (NCO) to enable use of a two-component syringe equipped with a static mixer to mimic ARE printing. pMDI (5.6 g, 14.4 mmol) and FS (0 [0.0 wt%], 0.13 g [2.5 wt%], 0.26 g [5.0 wt%], or 0.39 g [7.5 wt%]) were added to a scintillation vial and rigorously mixed using a high-velocity vortex mixer; pMDI and FS mixture was then syringed into one cartridge of the dual-component syringe (Sulzer Mixpac AA 050-01-10-01). DBTDL (0.032 g, 0.05 mmol) was added to a separate scintillation vial using a micropipette. PTMEG (3.0 g, 3 mmol), BD (1.4 g, 15.8 mmol), and FS (0 [0.0 wt%], 0.13 g [2.5 wt%], 0.26 g [5.0 wt%], or 0.39 g [7.5 wt%]) were subsequently added to the scintillation vial, then mixed using a high-velocity vortex mixer, prior to syringing the mixture into the second cartridge of the dual component syringe. Care was taken to minimize trapped air when loading each cartridge; prior to each experimental characterization, air was evacuated by individually compressing each cartridge until no voids were present. Sulzer Mixpac static mixers (MAH 03-16S) were used for all experimental studies.

2.3 Preparation of Polyurethanes for In Situ Polymerization and 3D Printing

A Hyrel 3D Engine SR FFF printer fitted with a Hyrel 3D SMH-2 Extruder was adapted to accommodate a multicomponent reactive liquid feed system to prepare a series of filled and unfilled PUs for this research. A simplified schematic is provided in Figure 2; the physical lab-scale ARE printer is shown in Figure A-1. A

two-component approach was used to synthesize/print PUs where the OH component was composed of premixed stoichiometric amounts of polyol, chain extender, and catalyst while NCO was composed of only the isocyanate. Two Cole Parmer Masterflex Easy-Load L/S peristaltic pumps paired with flexible Saint Gobain Tygon PVC S3 tubing were used to supply reactive material to the manifold with static mixer. Tubing with 3/32-inch inner diameter (ID), 7/32-inch outer diameter (OD) was used to supply OH, while larger-diameter tubing (1/8-inch ID, 1/4-inch OD) was used to supply NCO at a higher flow rate. Tubing was affixed to the SMH-2 Extruder via 1/8-inch hose ID barbed fittings. Disposable Sulzer Mixpac MAH 03-17S static mixers (16 mixing elements, 3.2-mm ID, and 74 mm overall length) were used as the static mixers for all PU prints.

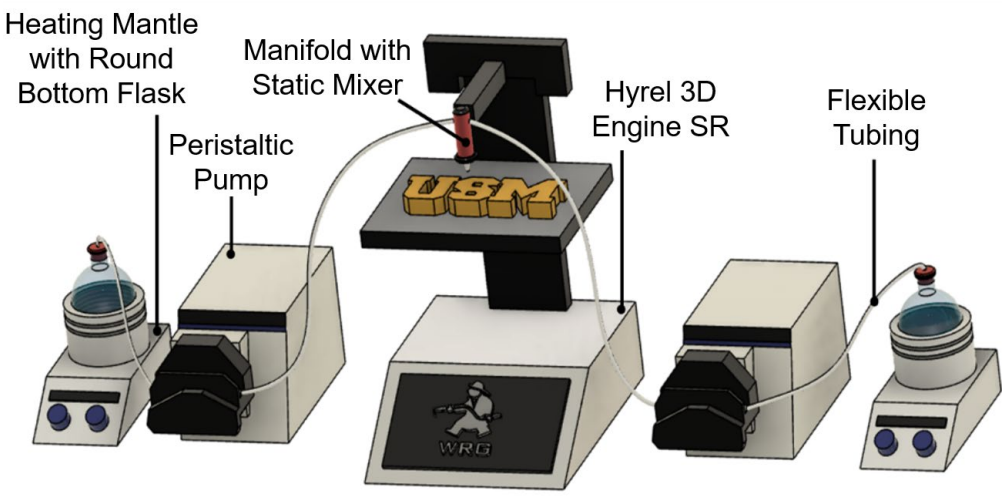

Figure 2. Lab-scale ARE 3D printing assembly utilizing two peristaltic pumps and modified Hyrel 3D Engine SR.

In a typical reaction, DBTDL (600 ppm tin, 1.27 g, 2.02 mmol), BD (57.07 g, 633.21 mmol), PTMEG (119.62 g, 119.62 mmol), and FS (10.5 g) were added to a flame-dried, one-neck 500 mL round-bottom flask to prepare the OH component. The mixture was blended rigorously with an overhead mixer to distribute the fumed silica. A dried stir bar was then added to the mixture, heated to 60 °C, and degassed overnight. Prior to printing, the mixture was cooled to 25 °C and stirred continuously throughout the print to ensure homogeneous mixing. pMDI (222.04 g, 575.69 mmol) and FS (10.5 g) were added to a separate flame-dried 500-mL round-bottom flask to prepare the NCO component. The mixture was blended rigorously with an overhead mixer to distribute the fumed silica prior to adding a dried stir bar and degassing overnight at 25 °C. An isocyanate index of [NCO]/[OH] = 1.03 and 5.0 wt% FS was targeted, thus the pumps were calibrated to a mass flow ratio of 0.81 (OH):1 (NCO). Calibration was achieved by determining the mass of deposited material in a 30-s period to determine mass flow rates; a minimum of

three pump settings were evaluated, and mass flow rates were determined a minimum of three times to establish an average of each trial. While printing, both OH and NCO were held at a constant temperature of 25 °C in Chemglass Digital Magnetic Hot Plate Stirrers with 500-mL Optitherm Reaction Blocks.

2.4 Rheological Experiments

A TA Instruments ARES G2 rheometer operated in a strain-control mode with 25-mm-diameter aluminum parallel plates, and a 1-mm constant gap was used for all experiments. Small amplitude oscillatory shear experiments were performed at 25 °C, 10 rad/s, and 1% strain. A Sulzer Mixpac dual-component syringe (AA 050-01-10-01) with 1:1 volumetric cartridges equipped with Sulzer Mixpac static mixer (MAH 03-16S) was used to deposit reactive material directly onto the parallel plates. Reactive materials were separated until extrusion through the static mixer to deposit material directly on the parallel plates; this corresponded to approximately 30 s between mixing and experimental start. Flow sweeps from 1 to 100 s^{-1} at 25 °C were performed to study the influence FS loading level on monomeric viscosities. Frequency sweeps from 10^{-2} to 10^{2} rad/s at 25 °C were conducted to observe the elastic and viscous response of monomers.

2.5 Real-Time Fourier Transform Infrared Spectroscopy

In situ tracking of all PU reaction progressions was performed in the spectral range of 600–4000 cm^{-1} on a PerkinElmer Frontier IR spectrometer in transmission mode with a 10° transmission accessory from Pike Technologies using sodium chloride (NaCl) plates at ambient conditions. Spectra were co-averaged over 10 scans at 2 cm^{-1} resolution for an average of approximately 11 s per scan. Peaks indicative of PU polymerization were tracked at the following wave numbers: 3500 cm^{-1} (primary alcohol), 3300 cm^{-1} (secondary amine), and 2260 cm^{-1} (isocyanate functionality), all referenced to C-H stretching observed from 2800 to 3100 cm^{-1} to normalize the results. The degree of conversion (DOC) for each polymerization was determined using Equation 1, where A_t is the normalized area under the isocyanate peak at t and A_0 is the normalized area under the isocyanate peak at experimental start.[25] Reactive PUs were syringed directly onto the NaCl plate and spread into a thin film using a razor blade prior to experimental start.

$$DOC = \left(1 - {}^{A_t}/_{A_0}\right) * 100\% . \quad (1)$$

3. Results and Discussion

3.1 Chemorheological Considerations of Polyurethanes for Reactive AM

Successful ARE printing is dependent on achieving balanced chemorheological properties, which encompass viscoelastic behavior of the reacting material as it transitions from the monomeric to polymeric state.[26] Monomer reactivity is important for controlling fast cure kinetics, high initial viscosity, and adequate modulus at deposition. Deposited, partially cured material must develop gel strength rapidly (on the time scale of print speed) to prevent initial layers from sagging under the weight of subsequent layers. This resistance to sag, herein referred to as dimensional stability, is defined as the ability of the reacting material to retain its intended geometric shape upon deposition, resisting flow (in the X, Y-directions), and sag (in the Z-direction). Theoretically, this would correspond to a critical zero-shear viscosity (to reduce significant flow at deposition) and a critical storage modulus (G', to support subsequently deposited layers). These values are also heavily influenced by the DOC at deposition, where it is well established that viscosity increases with increasing molecular weight.[26] A further consideration is that the reactive monomer polymerization must also have a gel time longer than the residence time of the mixing nozzle to avoid gelation within the static mixer print head. High DOCs may also result in a diffusion-limited specimen that is spatially locked and unable to react further,[27] which implies that a system-dependent critical extent of reaction exists. Above the critical DOC, minimal interlayer polymerization is expected, thus decreasing achievable isotropic properties. When considering these implications for dimensional stability and mechanical anisotropy, the window for acceptable chemorheological properties narrows (Figure 3). Ultimately, print-processing parameters, such as print speed (as it relates to time between each deposited layer) and polymer design can be leveraged to navigate this window, thus influencing the DOC of deposited layers.

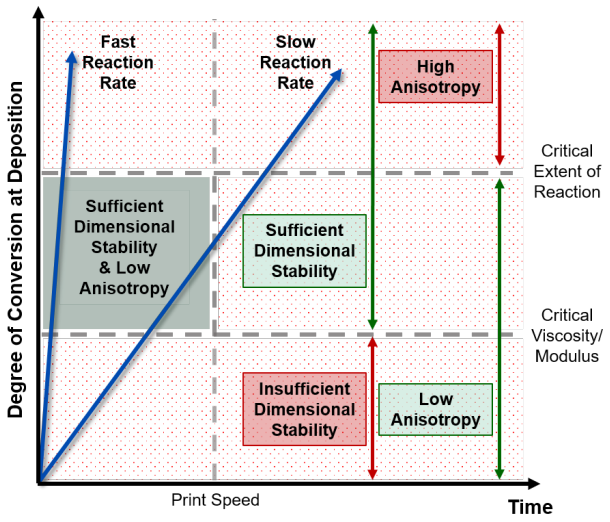

Figure 3. Idealized ARE printability requirements depicting critical viscosity/modulus for attaining dimensional stability, critical extent of reaction for reducing mechanical anisotropy, and idealized window for achieving both on a time scale commensurate with print speed that can be targeted through kinetic control.

3.2 Evaluation of Monomer Processability for ARE

Rheological shear sweeps at ambient conditions were performed on each individual component (NCO or OH functionality) containing various FS loading levels to determine reasonable FS concentrations for processability (Figure 4). FS was added on a weight basis of each reactive component (NCO or OH), where viscosity increased with increased FS concentration. Differences in rheological responses between the two components were observed, where the OH component containing 5+ wt% demonstrated shear thinning behavior, attributed to silica gel formation, resulting from particle–particle hydrogen bonding.[28]

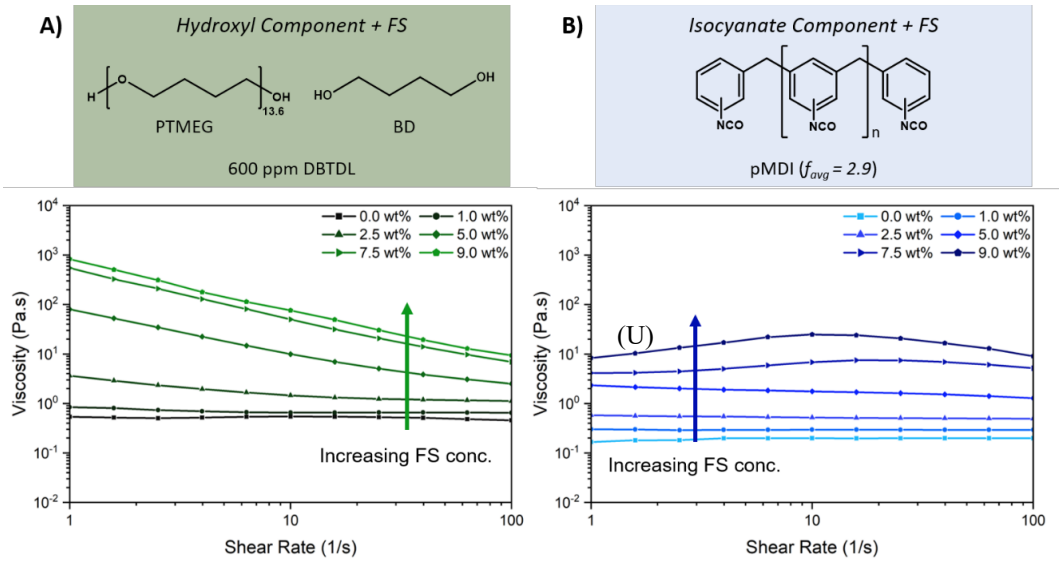

Figure 4. Rheological shear sweeps depicting FS influence on reactive components: (A) hydroxyl components and (B) isocyanate component.

3.3 Chemorheological and Spectroscopic Studies of Fumed Silica-Containing Polyurethanes

A two-component syringe, with one cartridge filled with pMDI and the other filled with OH components, was equipped with a static mixer to mimic the feed strategy for ARE printing. Qualitative evaluation of FS influence on dimensional stability was obtained by observing differences in flow and height while dispensing FS-PUs onto a Kapton film (Figure 5). An increased FS loading level resulted in an increase in vertical height and change in shape.[29] Substantial dimensional stability was observed in the 7.5 and 9.0 wt% FS PUs, as they retained the shape of the static mixer nozzle. However, it was hypothesized that an ideal FS concentration was between 5.0 and 7.5 wt% to allow adequate diffusion and interaction between layers for maximized interlayer polymerization.

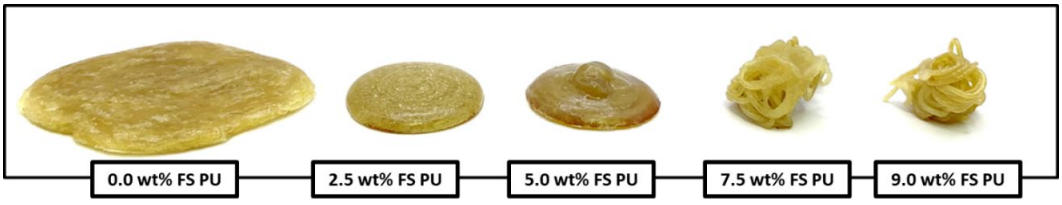

Figure 5. PUs prepared from two-component syringe containing increasing amounts of FS, demonstrating increased dimensional stability with increasing FS.

In situ chemorheological properties were quantitatively characterized using the two-component syringe to deposit stoichiometric quantities of NCO/OH directly onto the parallel plates (Figure 6). Use of the two-component syringe minimized

time between the onset of polymerization and experimental data collection, enabling comparison of chemorheological results to PU print quality and characteristics. Initial attempts to characterize 9.0 wt% PUs were unsuccessful due to high viscosities that limited processability. Results for the 0.0 to 7.5 wt% FS PUs are tabulated in Table 1. Initial storage modulus (G'_0) was observed to increase with increasing FS concentration. Notably, G'_0 values were larger than initial loss modulus (G''_0) values for 5.0 and 7.5 wt% FS PUs, which indicated PUs were initially elastically dominated.[30] This behavior was not observed in 0.0 and 2.5 wt% FS PUs; rather, G''_0 is greater than G'_0 for these samples, which is typical for reactive materials transitioning from a viscous monomeric state to an elastic polymer. The initial elastic behavior observed in 5.0 and 7.5 wt% FS PUs was attributed to the initial formation of physical gels composed of silica particles interconnected through weak physical bonds. However, these gel times did not translate to dimensional stability, and future work includes further investigation into this unexpected trend.

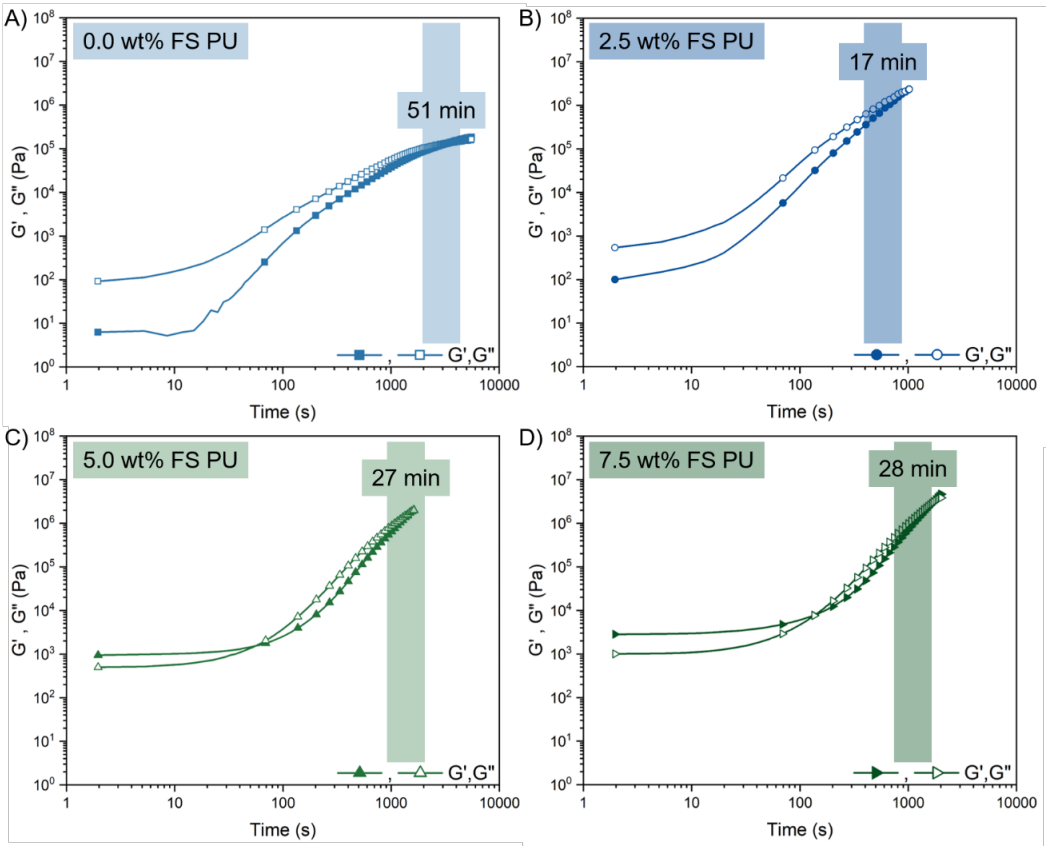

Figure 6. Chemorheological responses of PUs containing (A) 0.0 wt% FS, (B) 2.5 wt% FS, (C) 5.0 wt% FS, and (D) 7.5 wt% FS.

Table 1. Rheological results of FS-containing PUs.

PU sample (wt% FS PU)	G'$_0$ (Pa)	G"$_0$ (Pa)	G'$_0$/ G"$_0$	η_0 (Pa·s)	G'/G" crossover (min)
0.0	6	92	0.07	9	51
2.5	100	539	0.19	55	17
5.0	942	500	1.88	107	27
7.5	2832	1003	2.82	300	28

PU reactivity was observed via real-time Fourier transform infrared (RT FTIR) by monitoring consumption and formation of crucial chemical moieties. A representative spectra of 2.5 wt% FS PU is shown in Figure 7A, where a distinct decrease in isocyanate intensity at 2260 cm^{-1} was observed as time progressed. Spectra of the remaining FS PUs are provided in Figure A-3. DOC as a function of time is provided in Figure 7B, where the inset figure denotes the first 2 min of reaction. Due to the delay between initial formulation mixing and FTIR experimental start time, only final DOCs are provided in Table 2 and increased with increasing FS concentration.

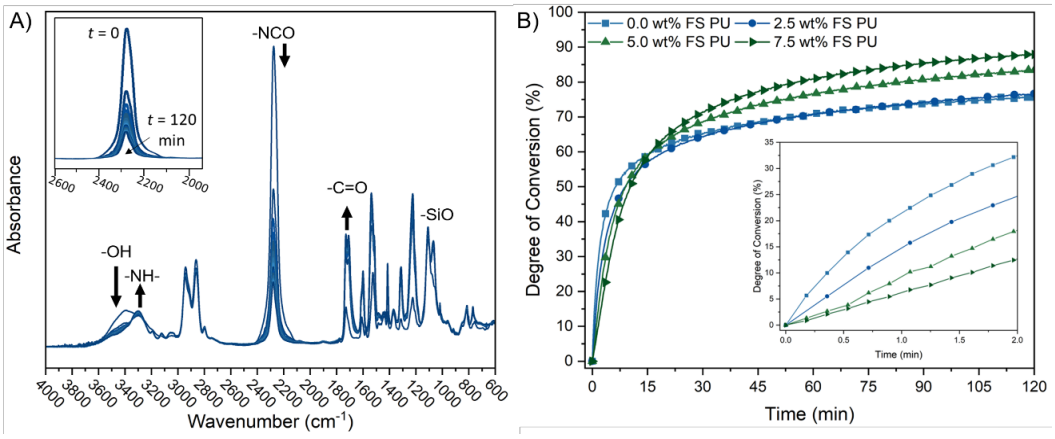

Figure 7. (A) Representative RT FTIR spectra for 2.5 wt% FS PU over 2 h. (B) Degree of conversion vs. time obtained via RT FTIR for FS-containing PUs. Inset figure highlights the differences in initial rate of reactions.

Table 2. FS-PU rate of reaction and final degree of cure

Sample (wt% FS PU)	Final DOC at 2 h (%)
0.0	75.6 ± 3.9
2.5	76.7 ± 1.7
5.0	83.4 ± 5.2
7.5	87.9 ± 7.4

Lower initial rates of reaction for the FS-containing PUs were attributed to decreased diffusivity of the reactive components due to the increased viscosity of the reaction medium. This is observed in similar systems[31,32] and decreased concentration of reactive functionalities at higher FS concentrations. Surprisingly, final DOC was not affected by the initial delay in polymerization imparted by FS, as final DOC was observed to increase with increased FS concentration. This was attributed to the delayed polymerization in higher FS-containing samples yielding more leeway during sample preparation time—that is, less isocyanate was consumed prior to the start of the RT FTIR experiment, which enabled more consumption during the experimental progression (Figure A-4).

Through rheological and spectroscopic analysis, a relationship between FS loading level in PUs and processability was established, wherein higher loading levels led to a slower initial rate of reactions but higher final degree of cure. Leveraging FS loading levels undoubtedly allows for reactive PUs to reach the required dimensional stability and low anisotropy for successful ARE printing.

3.4 Simultaneous Polymerization and 3D Printing of Polyurethanes

Correlating rheological and spectroscopic results provide a pathway for elucidating and tailoring chemorheological properties to successfully print FS PUs via ARE. Namely, 0.0 wt% FS PUs had the highest initial rate of reaction but longest gel time, where we hypothesized that long gel times would lead to dimensional stability issues. Conversely, increasing FS concentrations in PUs led to faster gel times of 16, 27, and 28 min for 2.5, 5.0, and 7.5 wt% FS PUs, respectively. FS PUs with concentrations of 5.0 and 7.5 wt% demonstrated higher initial moduli and viscosities, despite slower gel times compared to 2.5 wt% FS PUs. However, 7.5 wt% FS was above processability limitations of the printing setup and therefore was not printed in this investigation. Our initial hypothesis that poor dimensional stability would be observed for the 0.0 and 2.5 wt% FS PUs, due to longer gelation times and lower initial viscosities/moduli, was demonstrated and can be observed in the appendix (see Figures A-5 and A-6).

For all subsequent print trials, 5 wt% FS PUs were used to examine the influence of increased initial viscosity/modulus, yet slower gelation time, on ARE printability. PU specimens were printed at 100 mm/s print speed according to a single-walled ovular geometry (Figure 8b). Printed specimen dimensions measured 80.6 mm long and 26.5 mm wide, with individual wall thicknesses of 4.60 mm; targeted geometry is provided in Figure 8a. Though measured dimensions were larger than targeted dimensions, 5.0 wt% FS PUs were capable of being

successfully printed with vertical heights greater than 25 mm. Optimization of reactive material properties, through increased initial viscosity and reactivity, is envisioned to further enhance print quality and better match targeted print dimensions. Small defects, namely the ripple along the bottom of the print, were attributed to pump inconsistencies; nonetheless, the deposited PU could sufficiently flow to overcome detrimental irregularities. Similarly, an optically lighter section was observed at the top of the print. This was attributed to trapped CO_2, as a result of side reactions between pMDI isocyanate and ambient moisture. The cross-sectional area was analyzed via optical microscopy to better observe voids and the layer regularity (Figure 9A), while ripples caused by flow inconsistencies were imaged via profilometry (Figure 9B, C). Of importance, no distinct layer boundaries were observed when analyzing the cross-sectional area, which indicated good consolidation of the reactive polymer across the layer–layer interface. This was further probed through scanning electron microscopy (SEM), where the vertical cross-section displays three layers with no distinct interface observed at the layer–layer boundary, further indicating coalescence of deposited layers (Figure 10). Moreover, no distinct FS agglomerates were observed. SEM energy dispersive X-ray (EDX) and elemental mapping were used to observe the distribution of Si throughout the print specimen (Figure 11). Elemental analysis indicated 60.2 wt% C, 8.2 wt% N, 26.4 wt% O, 4.7 wt% Si, and 0.2 wt% Al and an even distribution of Si throughout the imaged specimen.

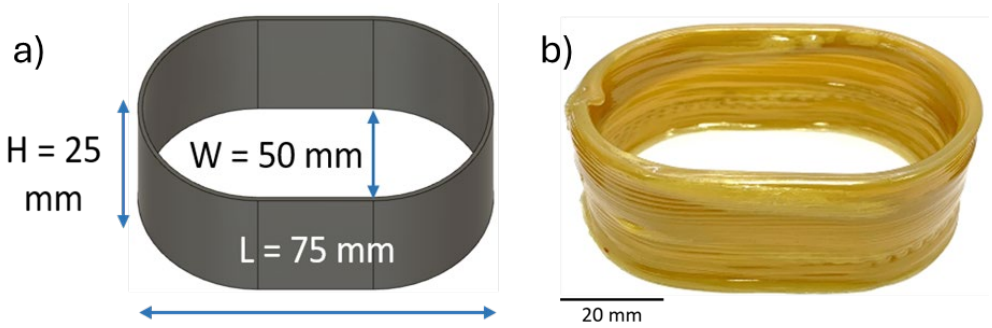

Figure 8. (a) Target print geometry and (b) demonstration of simultaneous polymerization and printing of 5.0 wt% FS PU using ARE.

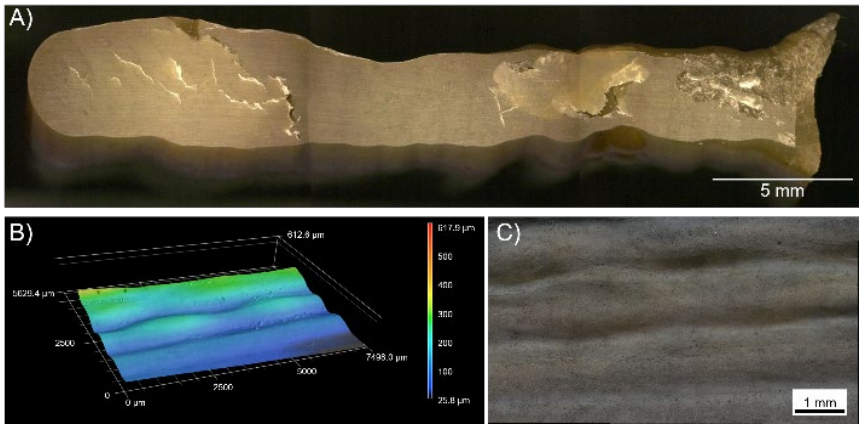

Figure 9. (A) Optical microscopy (OM) image depicting cross section of 5.0 wt% FS PU print specimen. Observed voids were attributed to isocyanate side reactions. No distinct layer boundaries were observed. Note: Two distinct vertical lines are present due to stitching of three OM images together. (B) 3D height and (C) optical maps of 5.0 wt% FS PU specimen.

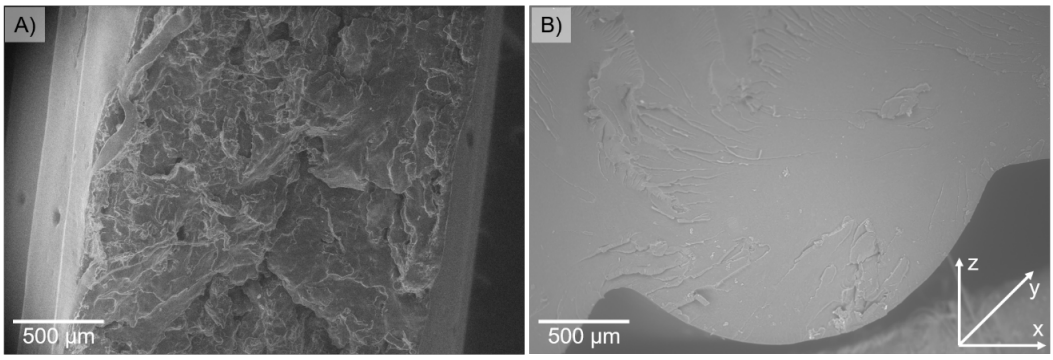

Figure 10. SEM images of (A) cross section of 5.0 wt% FS PU cryofractured at the layer–layer interface (vertically printed layers) and (B) cross section of 5.0 wt% FS PU specimen with layers transverse to surface.

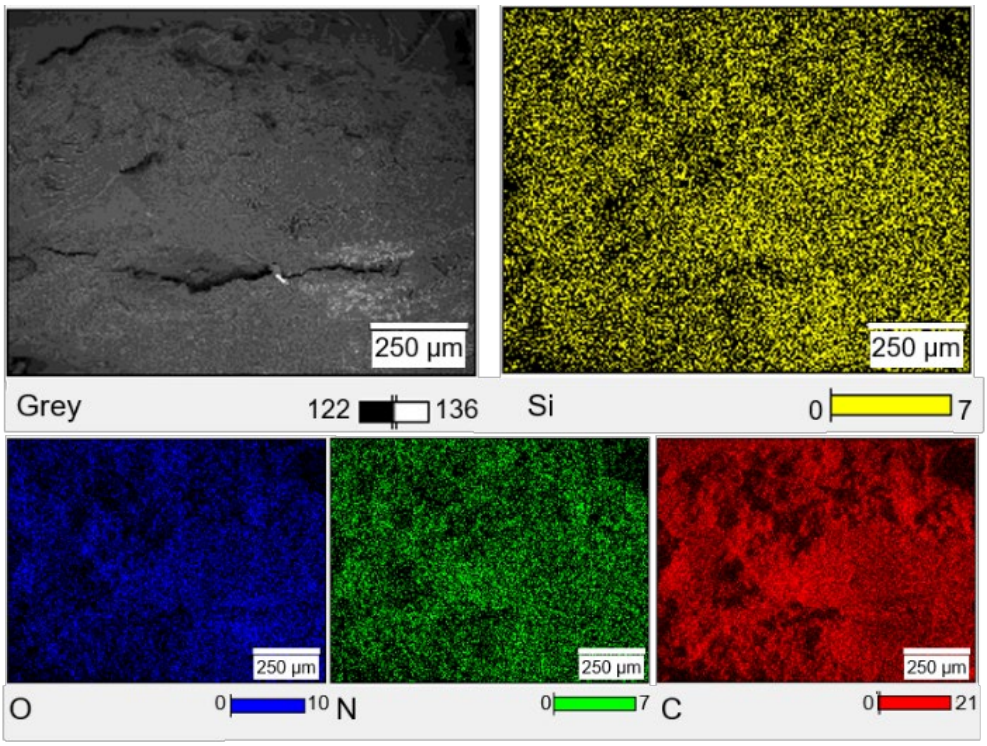

Figure 11. SEM EDX of 5.0 wt% FS PU depicting random distribution of Si in addition to mapping of O, N, and C.

FS loading levels were confirmed through thermogravimetric analysis (TGA) of the printed PUs (Figure 12A); samples were obtained from the top, middle, and bottom of the printed specimen to confirm the incorporation of FS across the entire print. An average loading level of 4.68 wt% was determined, where the residual weights at 900 °C ($Wt_{900\ °C}$) and onset of degradation ($T_{5\%}$), observed as the temperature at 5% weight loss, are provided in Table 3 for each sample. Good agreement was observed for both $T_{5\%}$ and $Wt_{900\ °C}$ between the top and middle specimens. The bottom samples had a lower $T_{5\%}$ and lower $Wt_{900\ °C}$, which was attributed to the equilibration of feeds over the duration of the print. All three specimens displayed similar degradation profiles to the unfilled PU (Figure A-8) with three primary degradation events occurring at approximately 315 °C, 425 °C, and 570 °C that correspond to hard segment degradation and decomposition of urethane bonds, degradation of the soft segment and ether linkages, and loss of remaining volatile material and residual char, respectively.[33,34] As-printed samples were analyzed with differential scanning calorimetry (DSC) to determine if samples were under-cured, where a small residual exotherm was observed at 176.4 °C (Figure A-9); therefore, specimens were post-cured at 160 °C for 2 h. Thermomechanical properties and glass transition temperatures (T_g's) of as-printed and post-cured specimens were obtained via dynamic mechanical analysis (DMA)

(Figure 12B). Both specimens displayed two peaks in Tan δ, as is typical of PUs displaying microphase separation, where the lower temperature Tan δ is indicative of the soft segment T_g ($T_{g,\,SS}$) and the peak in Tan δ observed at higher temperatures is representative of the hard segment T_g ($T_{g,\,HS}$).[34] Minimal differences were observed for $T_{g,\,SS}$ between the as-printed and post-cured samples, with T_g's of –75.9 °C ± 0.73 and –75.1 °C ± 0.36, respectively, which agreed well reported T_g's of PTMEG 1000 (–77 °C).[35] A slight increase from 67.9 °C ± 1.9 to 74.1 °C ± 1.6 in $T_{g,\,HS}$ was observed following the post-cure. Full width at half maximums were unable to be determined due to the sample yielding after traversing $T_{g,\,HS}$. While printed specimens required a post-cure to fully complete polymerization, the post-cure was minimal compared to similar printing methods that require elevated temperatures and cure times. Therefore, this study provided the first demonstration of simultaneous in situ polymerization and 3D printing of PUs, wherein specimens with vertical heights over 25 mm were achieved, with minimal postprocessing requirements.

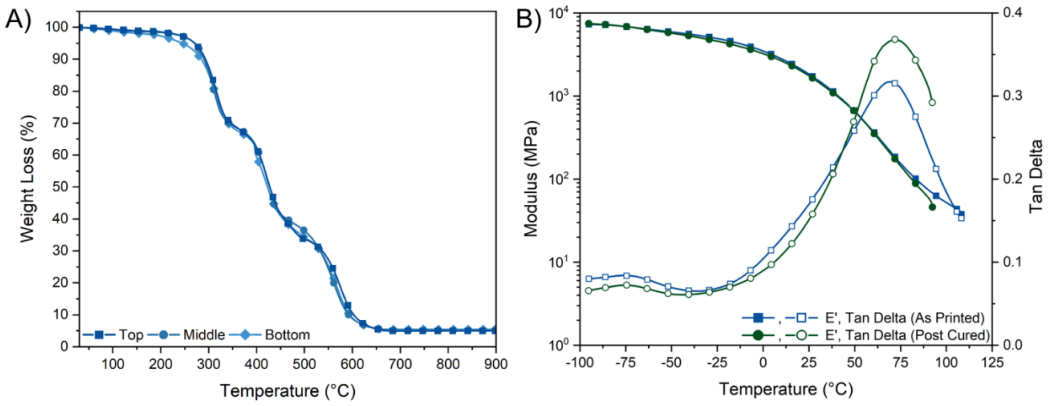

Figure 12. (A) Thermal degradation pathways of 5.0 wt% FS PU specimens from top, middle, and bottom of print. (B) DMA of as-printed and post-cured PU print.

Table 3. TGA results of ARE printed PU.

Sample	$T_{5\%}$ (°C)	$Wt_{900\ °C}$ (%)
Top	273 ± 2.6	4.93 ± 0.06
Middle	270.9 ± 0.40	5.00 ± 0.17
Bottom	248.9 ± 4.1	4.11 ± 0.66

4. Conclusion

Limitations of previous ARE literature reports were addressed by using a 1:1 dual-component syringe equipped with a static mixer and PU composition that corresponded to 1:1 volumetric feed ratios. Rheological characterization revealed 2.5 wt% FS PUs had the fastest gel time (16.7 min) and 0.0 wt% FS PUs had the slowest (51 min), while 5.0 and 7.5 wt% FS PUs had gel times of 27 and 28 min, respectively. While 0.0 and 2.5 wt% FS PUs did not form initial physical gels, 2.5 wt% FS PUs had the fastest gel time (16.7 min) and 0.0 wt% FS PUs had the slowest (51 min). Complex interfacial reactions between the FS and the PU components resulted in nonintuitive viscosity trends. RT FTIR results supported trends where initial rates of isocyanate consumption decreased with increased FS concentration.

PUs containing 5.0 wt% FS were simultaneously synthesized and printed, demonstrating consistent uniformity and agreement with targeted geometry, with vertical heights of 25 mm. Post-print analysis of specimen cross section indicated good coalescence of deposited layers, as no distinct layer-layer boundaries were observed. Moreover, through SEM and elemental mapping, Si was shown to be uniformly distributed throughout the specimen without distinct agglomerations, while TGA results indicated good incorporation of FS at 4.68 wt%. T_g's of as-printed and post-cured specimen were determined via DMA, where minimal differences in $T_{g,\,SS}$ was observed. A 6.2 °C increase in $T_{g,\,HS}$ was observed following a post-cure at 160 °C for 2 h, which indicated minimal postprocessing of printed specimens was required to drive polymerization to completion. This study demonstrated the ability to successfully simultaneously synthesize and 3D print PUs using ARE.

5. References

1. ASTM ISO/ASTM52900-21. Additive manufacturing: general principles, fundamentals, and vocabulary. ASTM International; 2022 Mar 2. https://www.iso.org/obp
2. Beaman JJ, Bourell DL, Seepersad CC, Kovar D. Additive manufacturing review: early past to current practice. J Manuf Sci Eng. 2020;142(11). https://doi.org/10.1115/1.4048193
3. Gardiner G. Big area additive manufacturing (BAAM): increasing material feed and speed. CompositesWorld. 2015 Mar 15.
4. Post BK et al. Big area additive manufacturing application in wind turbine molds. 28th Annual International Solid Freeform Fabrication Symposium - An Additive Manufacturing Conference, SFF 2017; 2017 Aug 7–9; Austin, TX.
5. Duty CE et al. Structure and mechanical behavior of big area additive manufacturing (BAAM) materials. Rapid Prototyp J. 2017;23(1):181–189. https://doi.org/10.1108/RPJ-12-2015-0183
6. Kishore V et al. Infrared preheating to improve interlayer strength of big area additive manufacturing (BAAM) components. Addit Manuf. 2017;14:7–12. https://doi.org/10.1016/j.addma.2016.11.008
7. Ahn SH, Montero M, Odell D, Roundy S, Wright PK. Anisotropic material properties of fused deposition modeling ABS. Rapid Prototyp J. 2002;8(4):248–257. https://doi.org/10.1108/13552540210441166
8. Calvert P, Liang Lin T, Martin H. Extrusion freeform fabrication of chopped-fibre reinforced composites. High Perf Polym. 1997;9(4):449–456.
9. Compton BG, Lewis JA. 3D-printing of lightweight cellular composites. Adv Mater. 2014;26(34):5930–5935. https://doi.org/10.1002/adma.201401804
10. Rios O et al. 3D printing via ambient reactive extrusion. Mater Today Commun. 2018;15(June 2017):333–336. https://doi.org/10.1016/j.mtcomm.2018.02.031

11. Uitz O, Koirala P, Tehrani M, Seepersad CC. Fast, low-energy additive manufacturing of isotropic parts via reactive extrusion. Addit Manuf. 2021;41(Sep 2020):101919. https://doi.org/10.1016/j.addma.2021.101919

12. Akindoyo JO et al. Polyurethane types, synthesis and applications-a review. RSC Adv. 2016;6(115):114453–114482. https://doi.org/10.1039/c6ra14525f

13. Das A, Mahanwar P. A brief discussion on advances in polyurethane applications. Adv Ind Eng Polym Res. 2020;3(3):93–101. https://doi.org/10.1016/j.aiepr.2020.07.002.

14. Kütting M, Roggenkamp J, Urban U, Schmitz-Rode T, Steinseifer U. Polyurethane heart valves: past, present and future. Expert Rev Med Devices. 2011 Mar:227–233. https://doi.org/10.1586/erd.10.79

15. Tailor-made Desmopan TPU for ski boot applications. Covestro AG; c2024 [accessed 2024 Sep 4]. https://solutions.covestro.com/en/highlights/articles/stories/2021/desmopan-for-ski-boot-applications

16. Farzan A et al. 3D scaffolding of fast photocurable polyurethane for soft tissue engineering by stereolithography: influence of materials and geometry on growth of fibroblast cells. Eur Polym J. 2020;139. https://doi.org/10.1016/j.eurpolymj.2020.109988

17. Zheng M et al. Direct ink writing of recyclable andin siturepairable photothermal polyurethane for sustainable 3D printing development. J Mater Chem A Mater. 2021;9(11):6981–6992. https://doi.org/10.1039/d0ta11341g

18. STRATASYS FDM TPU 92A BEST PRACTICES. http://articles.stratasys.com/user-guides/fdm-3d-printers/f123-series-

19. Semsarzadeh MA, Navarchian AH, Morshedian J. Reactive extrusion of poly(urethane-isocyanurate). Adv Polym Technol. 2004;23(3):239–255. https://doi.org/10.1002/adv.20014

20. Hyun ME, Kim SC. A study on the reactive extrusion process of polyurethane. Polym Eng Sci. 1988;28:743–757.

21. Tzoganakis C. Reactive extrusion of polymers: a review. Adv Polym Technol. 1989;9(4):321–330.

22. Lee LJ. Polyurethane reaction injection molding: process, materials, and properties. Rubber Chem Technol. 1980;53(3):542–599. https://doi.org/10.5254/1.3535053

23. Kröber P, Delaney JT, Perelaer J, Schubert US. Reactive inkjet printing of polyurethanes. J Mater Chem. 2009;19(29):5234–5238. https://doi.org/10.1039/b823135d

24. Müller M, Huynh QU, Uhlmann E, Wagner MH. Study of inkjet printing as additive manufacturing process for gradient polyurethane material. Prod Eng. 2014;8(1–2):25–32. https://doi.org/10.1007/s11740-013-0504-0

25. Tilly JC et al. Spectroscopic and rheological cross-analysis of polyester polyol cure behavior: role of polyester secondary hydroxyl content. ACS Omega. 2019;4(1):932–939. https://doi.org/10.1021/acsomega.8b02766

26. Halley PJ, George GA. Chemorheology of polymers: from fundamental principles to reactive processing. Cambridge University Press; 2009.

27. Osswald T, Rudolph N. Polymer rheology: from molecular structure to polymer process. Carl Hanser Verlag; 2013.

28. Raghavan SR, Walls HJ, Khan SA. Rheology of silica dispersions in organic liquids: new evidence for solvation forces dictated by hydrogen bonding. Langmuir. 2000;16(21):7920–7930. https://doi.org/10.1021/la991548q

29. Barthel H, Rösch L, Weis J. Fumed silica - production, properties, and applications. Organosilicon chemistry set: from molecules to materials. Wiley; 2005:761–778. https://doi.org/10.1002/9783527620777.ch91a

30. Xu B, Song YH, Zheng Q. Molecular relaxation and rheological behaviors of fumed silica/low-molecular weight polyethylene glycol suspensions. Acta Polymerica Sinica. 2017;(11):1832–1840. https://doi.org/10.11777/j.issn1000-3304.2017.17008

31. Lipatov YS, Kosyanchuk LV, Nesterov AE, Antonenko OI. Filler effect on polymerization kinetics and phase separation in polymer blends formed in situ. Polym Int. 2003;52(5):664–669. https://doi.org/10.1002/pi.937

32. Chiou B-S, Raghavan SR, Khan S. Effect of colloidal fillers on the cross-linking of a UV curable polymer gel point rheology and the winter chambon criterion. Macromolecules. 2001;34:4526–4533. https://doi.org/10.1021/ma010281a

33. Petrovic ZS, Zavargo Z, Flynn J, Macknight W. Thermal degradation of segmented polyurethanes. J Appl Polym Sci. 1994;51(6):1087–1095. https://doi.org/10.1002/app.1994.070510615

34. Prisacariu C. Polyurethane elastomers: from morphology to mechanical aspects. Springer Vienna; 2011. https://doi.org/10.1007/978-3-7091-0514-6

35. Expand your success on elastomers: PolyTHF. BASF; c2024 [accessed 2024, Sep 4]. https://chemicals.basf.com/dam/jcr:1c4a01a8-ff6a-36bb-9eed-830a52a19a7d/basf/chemicals/global/intermediates/brochues-for-special-applications/PolyTHF%20Leaflet_english.pdf

Appendix. Supplemental Printing Parameters, Setup, and Information

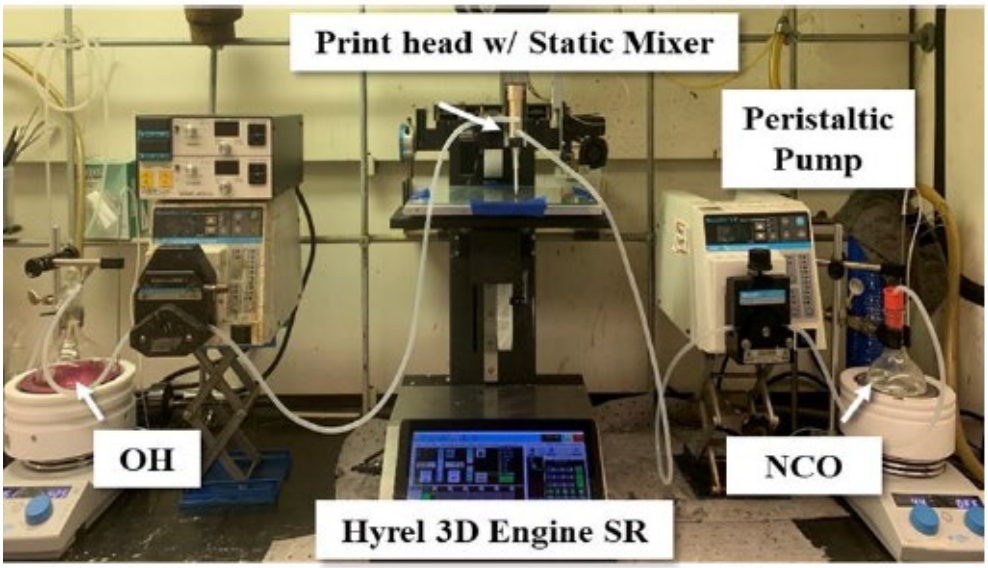

Figure A-1. Physical print platform used for this research.

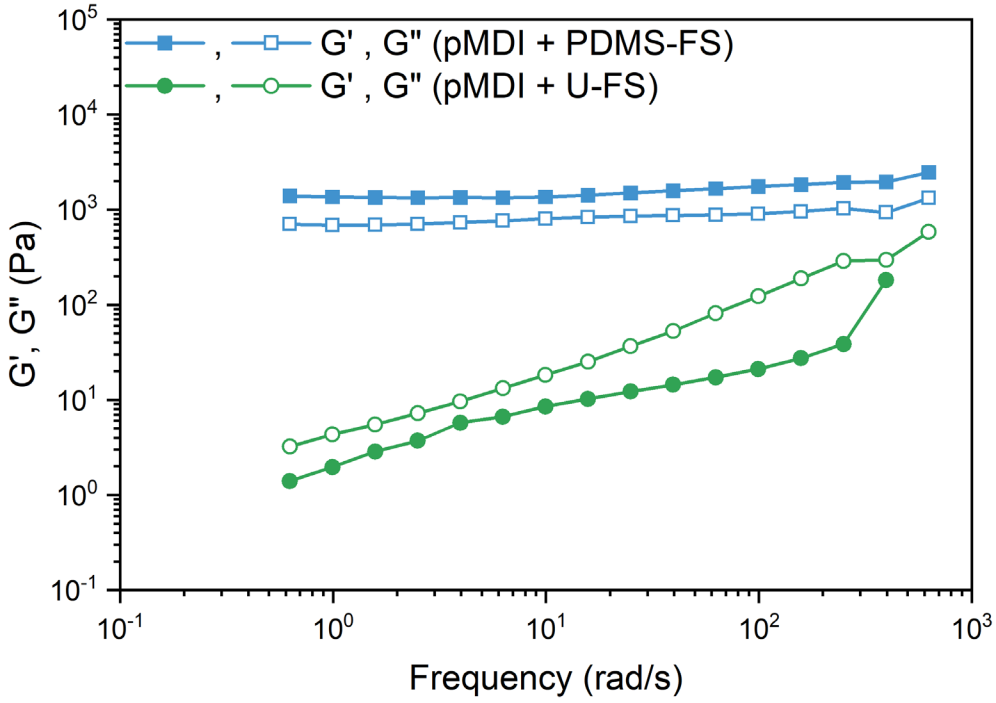

Figure A-2. Frequency sweep results of pMDI with PDMS-FS and U-FS, displaying silica gel formation for pMDI + PDMS-FS and silica sol formation in pMDI + U-FS.

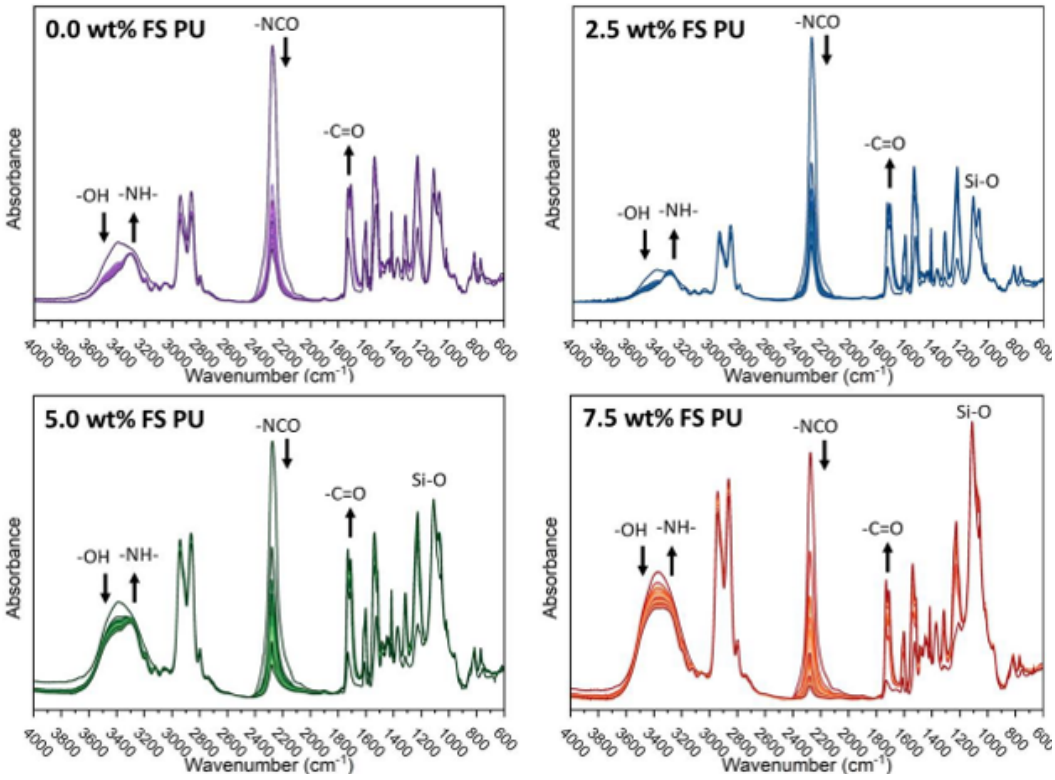

Figure A-3. RT FTIR spectra obtained over 2 h for all FS-containing PUs.

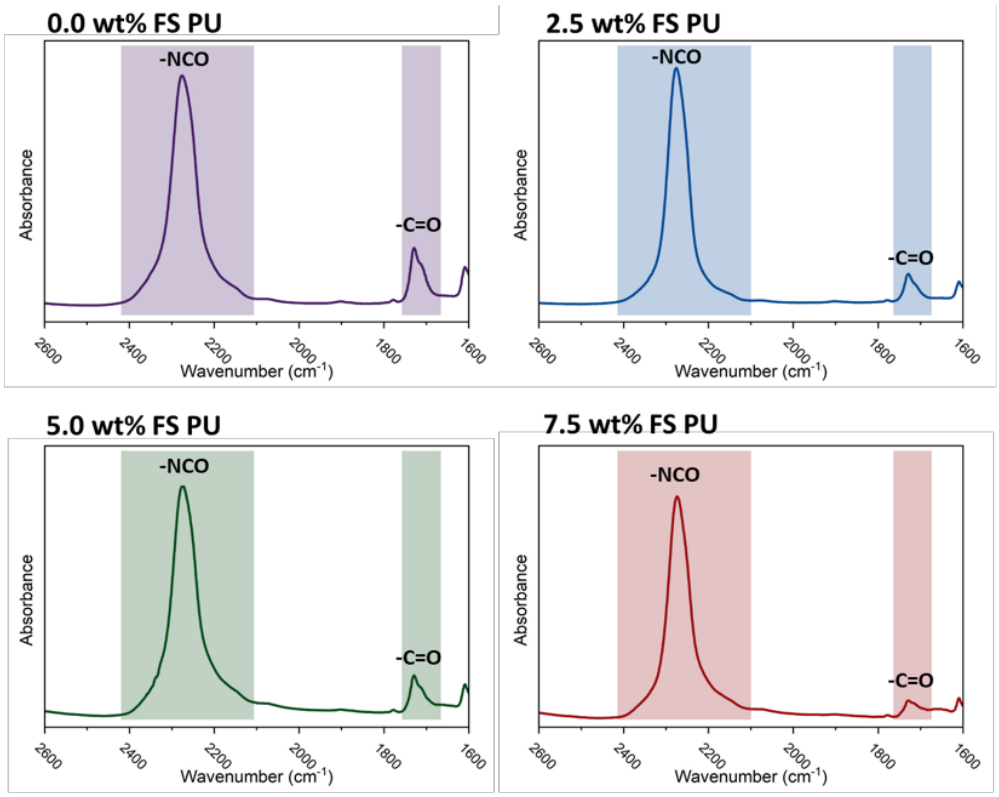

Sample	$Area_{NCO,\ t=0}$	$Area_{C=O,\ t=0}$	$Area_{C=O,\ t=0} / Area_{NCO,\ t=0}$ (%)
0.0 wt% FS PU	58.2	5.5	9.4
2.5 wt% FS PU	48.8	2.8	5.7
5.0 wt% FS PU	84.3	4.8	5.7
7.5 wt% FS PU	35.2	1.0	2.9

Figure A-4. First spectra (t = 0) of each PU sample depicting the presence of urethane carbonyl. Urethane carbonyl band intensity and percentage of initial urethane carbonyl area to initial isocyanate area decreased as FS concentration increased, which suggested a higher concentration of urethane linkages was formed during the sample preparation time.

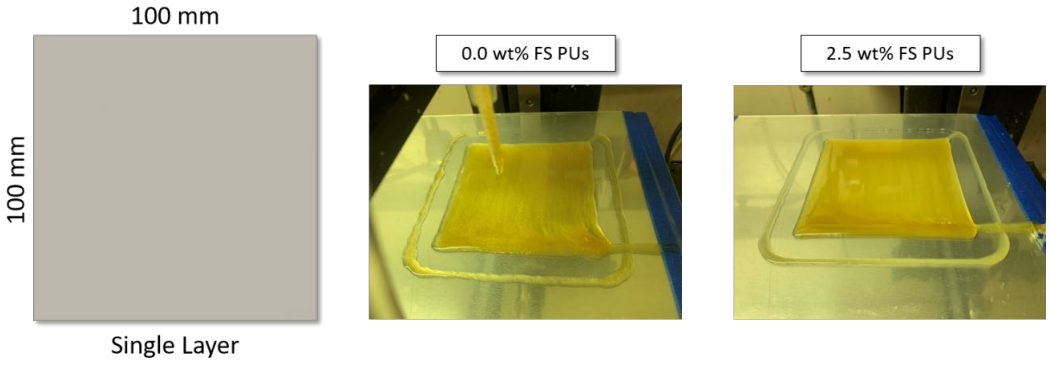

Figure A-5. (Left) Targeted single layer print geometry. (Middle) 0.0 wt% FS PU printed specimen according to left geometry; loss of shape retention highly apparent around corners. (Right) 2.5 wt% FS PU specimen printed according to targeted dimensions. Better shape retention compared to 0.0 wt% FS PU specimen.

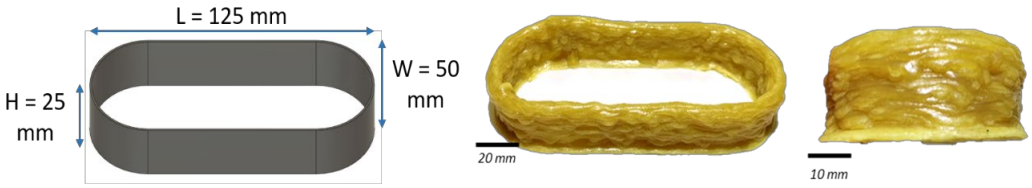

Figure A-6. (Left) Targeted single layer ovular print geometry. (Middle) Aerial view of 2.5 wt% FS PU printed specimen according to left geometry. (Right) Front view of 2.5 wt% FS PU specimen printed according to targeted dimensions. Significant "drips" indicated material did not have sufficient initial viscosity to prevent dripping and flowing upon deposition, despite 2.5 wt% FS PUs displaying the fastest gelation time observed rheologically.

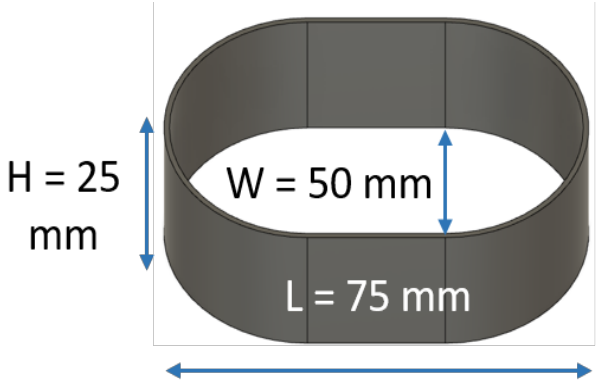

Figure A-7. Targeted single-walled ovular geometry.

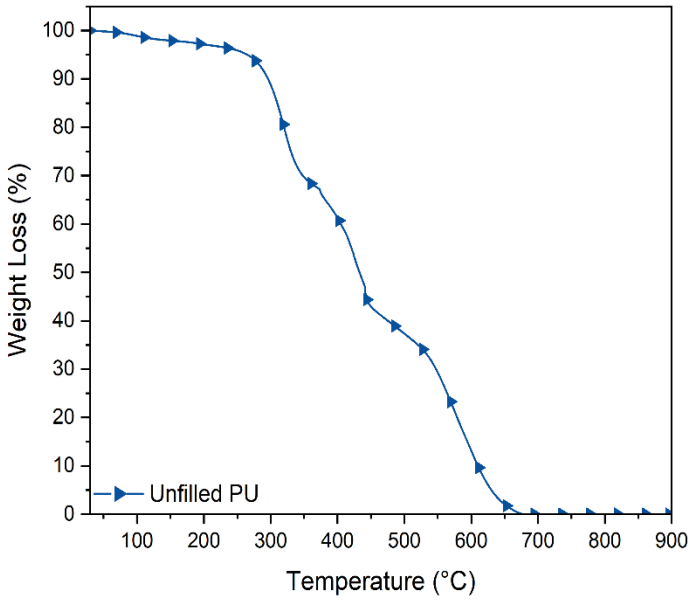

Figure A-8. Degradation profile of 0.0 wt% FS PU, depicting 0 wt% residual mass at 900 °C.

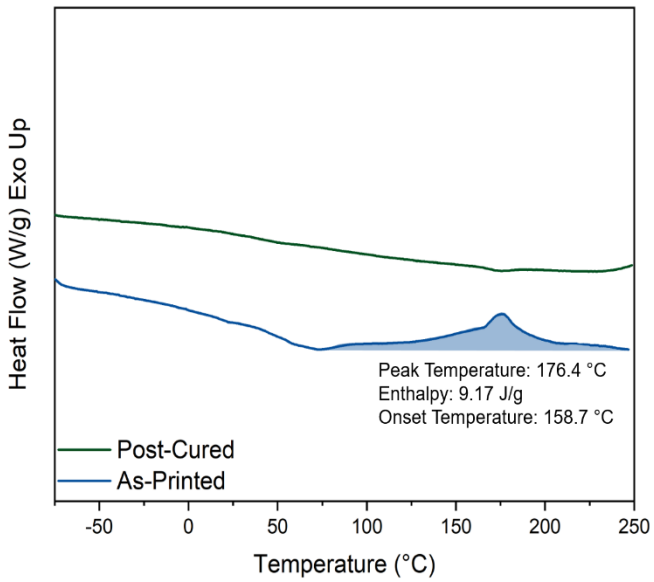

Figure A-9. DSC thermograms of as-printed and post-cured 5.0 wt% FS PU. Small residual exotherm observed at 176.4 °C with enthalpy of 9.17 J/g. Sample post-cured at 160 °C for 2 h prior to confirming no residual exotherm.

List of Symbols, Abbreviations, and Acronyms

3D	three-dimensional
AM	additive manufacturing
ARE	ambient reactive extrusion
BAAM	Big Area Additive Manufacturing
BD	1,4-butanediol
DBTDL	dibutyltin dilaurate
DIW	direct ink writing
DMA	dynamic mechanical analysis
DOC	degree of conversion
DSC	differential scanning calorimetry
EDX	energy dispersive X-ray
FFF	fused filament fabrication
FS	fumed silica
ID	inner diameter
IR	infrared
NaCl	sodium chloride
NCO	isocyanate
OD	outer diameter
OH	hydroxide
OM	optical microscopy
pMDI	polymeric 4,4'-diphenylmethane diisocyanate
PTMEG	polytetramethylene ether glycol
PU	polyurethane
RAM	reactive additive manufacturing
REX	reactive extrusion
RIM	reaction injection molding

RT FTIR	real-time Fourier transform infrared
SEM	scanning electron microscopy
SLA	stereolithography
T_g	glass transition temperature
TGA	thermogravimetric analysis
TPU	thermoplastic polyurethane

1 (PDF)	DEFENSE TECHNICAL INFORMATION CTR DTIC OCA
1 (PDF)	DEVCOM ARL FCDD RLB CI TECH LIB